RESONEUT: A detector system for spectroscopy with (d,n) reactions in inverse kinematics

L.T. Baby[a], S.A Kuvin[a,1], I. Wiedenhöver[a], M. Anastasiou[a], D. Caussyn[a], K. Colbert[b], N. Quails[b], D. Gay[b]

[a] *Florida State University, Department of Physics, Tallahassee, Fl 32306, USA*
[b] *University of North Florida, Department of Physics, Jacksonville, Fl 32224, USA*

Abstract

The RESONEUT detector setup is described, which was developed for resonance spectroscopy using (d,n) reactions with radioactive beams in inverse kinematics and at energies around the Coulomb barrier. The goal of experiments with this setup is to determine the spectrum and proton-transfer strengths of the low-lying resonances, which have an impact on astrophysical reaction rates. The setup is optimized for $l = 0$ proton transfers in inverse kinematics, for which most neutrons are emitted at backward angles with energies in the 80-300 keV range. The detector system is comprised of 9 p-terphenyl scintillators as neutron detectors, two annular silicon-strip detectors for light charged particles, one position-resolving gas ionization chamber for heavy ion detection, and a barrel of NaI-detectors for the detection of γ-rays. The detector commissioning and performance characteristics are described with an emphasis on the neutron-detector components.

Keywords: Low energy neutron detection; Charged particle detection; Silicon-strip detectors; Radioactive beams; Inverse kinematics; Neutron time of flight.

1. Introduction

One of the prominent current goals of experimental nuclear astrophysics is the determination of reaction rates relevant to explosive nucleosynthesis. In

[1] Department of Physics, University of Connecticut

particular, proton-capture (p,γ) reactions involving proton-rich radioactive nuclei play an important role in determining the time scale and nucleosynthesis outcome of novae and x-ray bursts. The most important information required to determine the thermonuclear (p,γ) rates is the energy spectrum of the low-lying resonances, and the respective resonance strengths. Even with the next-generation of advanced radioactive beam facilities and dedicated separators such as DRAGON[1] or SECAR[2], direct cross section measurements to many of the lowest resonances will remain difficult and supplemental or surrogate experiments will be needed to guide those studies.

Light-ion transfer reactions provide an alternative way to probe the relevant proton resonances, a quantitative method which has been used extensively to study the low lying states of light nuclei [3]. The (d,n) reaction in particular has properties which make it suitable to investigate the spectrum of the lowest proton resonances. In a $^{\mathrm{A}}\mathrm{Z}(\mathrm{d,n})^{\mathrm{A+1}}(\mathrm{Z}+1)$ reaction, a proton is transferred from the deuteron to the ^{A}Z nucleus, connecting the same states as the captured proton in the $^{\mathrm{A}}\mathrm{Z}(\mathrm{p},\gamma)^{\mathrm{A+1}}(\mathrm{Z}+1)$ reaction, but with much larger reaction cross sections. The (d,n) reaction has a relatively small negative Q-value for the low-lying proton-resonances, starting with a value of Q=-2.22 MeV at the proton-emission threshold. These Q values are favoring the population of proton resonances with low angular momentum, which leads to a high sensitivity for the resonances of astrophysical interest.

The cross sections and angular distributions of (d,n) reactions are successfully reproduced by distorted wave born approximation(DWBA) theory [3], which allows to parameterize the cross section in spectroscopic factors. In normal kinematics with a deuteron beam bombarding a heavier target, low-angular-momentum transfer reactions will produce a neutron distribution peaked at “forward” angles, as illustrated in the left panel of Figure 1. The right panel of Figure 1 shows the angular distribution in the laboratory system and in inverse kinematics, with a heavier beam bombarding a target containing deuterium. The maximum neutron yield for the same reaction will occur at beam-“backward” directions, which poses both a challenge and opportunity for experiments.

In this paper we describe a compact experimental setup optimized for the spectroscopy of (d,n) reactions in inverse kinematics with radioactive beams at energies around the Coulomb barrier. In addition to neutron-detector systems, the setup contains silicon double sided strip detectors (DSSD) for light charged particles, a high-rate capable ion chamber for the detection of heavy reaction residues and a surrounding "barrel"-shaped setup of NaI scintillators for the coincident detection of γ–rays. The goal of experiments with this setup is to establish the spectrum of low-lying proton resonances and the bound states close to the proton-threshold and measure their cross sections with the aim to determine thermal (p, γ) reaction rates in astrophysical environments.

2. Design parameters of the RESONEUT setup

2.1. Kinematics, energy resolution, efficiency and background suppression requirements

In the following, we are discussing the properties of an experiment with the ^{12}C(d, n)^{13}N reaction in inverse kinematics, and a beam of ^{12}C at 56 MeV or 4.67 MeV/u, populating the 2.365 MeV excited state of spin-parity $1/2^+$ in ^{13}N. This state is an $l = 0$ proton-resonance at 422 keV c.m. resonance energy. The kinematic conditions are very similar to the studies of low-lying resonances with radioactive beams for which this device has been designed.

Most of the (d,n) neutrons are emitted in backward directions with energies in the 150-200 keV range, which are difficult to detect with most existing detector systems. However, if a detection scheme for neutrons of the required energy range is available, the kinematic conditions can be utilized in the design of a relatively simple, yet efficient experimental setup. First, the low neutron energies and the velocities between 0.5 cm/ns to 0.7 cm/ns allow to perform time-of-flight(TOF) measurements with a relatively high precision over a small flight path. Second, the neutron angular distribution of $l = 0$ proton-transfer reactions, which peaks between 0° and 25° in the center-of-mass system, translates to laboratory angles 180° - 120° in inverse kinematics. Third, the neutron z-velocities emitted from a given state exhibit a very slow variation with the angles in the relevant range, as displayed in the left panel of Figure 2. This observation implies that a simple wall-like setup of detectors at a constant z-coordinate upstream of the target generates a TOF spectrum, that can achieve good energy reconstruction with a very modest angular resolution, as displayed in the right panel of Figure 2.

For the experiments in question, an excitation-energy resolution of 200 keV FWHM is acceptable. Given the kinematic dependence of the TOF signal on the excitation energy displayed in Figure 2, this can be achieved from an experiment setup with a 10% FWHM TOF resolution, which corresponds to around 30 keV FWHM resolution on a typical detected neutron of 150 keV energy. Given the 2.5 cm thickness of the detector crystals described below, the flight-path uncertainty will the limiting factor in placing the detector systems in a compact geometry close to the target. We chose to place the detector systems in a wall-like setup at a z-coordinate 23 cm upstream from the target, which leads to ±5% uncertainty of in the flight path, the dominant factor limiting the Q-value resolution. Additional factors determining the experimental resolution will be discussed in Section 3.5.

The overall detection efficiency is another crucial parameter in the design of radioactive-beam experiments. A typical experiment maintains a beam of radioactive particles with intensities around 10^4 per second over several days. Deuterated polyethylene foils of around 0.5 mg/cm^2 density will be used as target, a value limited by the energy resolution requirements described above. Under such conditions a resonance populated at 100 mbarn total cross section would lead to 3300 reaction events per day. Therefore, in order to perform meaningful spectroscopy, the detector systems are required to have a total detection efficiency of several percent.

Another crucial factor in the design of our experiments is in the ability to detect the rare signals over a much stronger background of natural and laboratory-induced radiation levels. In the case of the in-flight radioactive-beam facility

RESOLUT, the beam-production target and the secondary target are located in the same room and hence significant levels of background radiation are present during the experiments. This beam-induced background radiation is essentially isotropic and the corresponding count rate will be approximately proportional to the active detector area. Therefore a compact detector setup close to the secondary target is favored to improve the signal-to-background ratio, as well as an active discrimination between neutron– and γ–induced events.

As an example for the magnitude of background suppression required, we note that during the first successful radioactive-beam experiment with the the RESONEUT setup using the $^{17}\mathrm{F}(d,n)$ reaction [7], the nine neutron-detector systems created around 3000 triggers per second, while the signal of interest amounted to a total of a few counts per day, a signal-to-background ratio of around 10^{-9}. This challenging environment led to the design of a compact detector system for the coincident detection of all reaction products, which we describe in the following sections.

2.2. Design of the RESONEUT *detector system.*

We display a schematic cross section of the RESONEUT setup in Figure 3. A design representation and a photograph of the setup are displayed in Figure 4. The setup is installed at the RESOLUT[4] radioactive experimental facility at the John D. Fox Superconducting accelerator facility at Florida State University.

As neutron detectors, RESONEUT employs 9 p-terphenyl crystals located at a constant beam-axis coordinate about 23 cm upstream from the target. Their characterization is the main purpose of this work. The detector systems are mounted outside of the vacuum chamber, in pockets cut out of a solid aluminum plate, which allowed to minimize the material in front of the detectors in an effort to reduce scattering by passive material around the detectors. The detector housing can be used with up to 16 detector systems.

Reaction events populating states above the proton threshold will lead to emission of a proton, whereas population of bound states will lead to γ-ray emission. Coincidence measurements of either reaction product and the recoiling

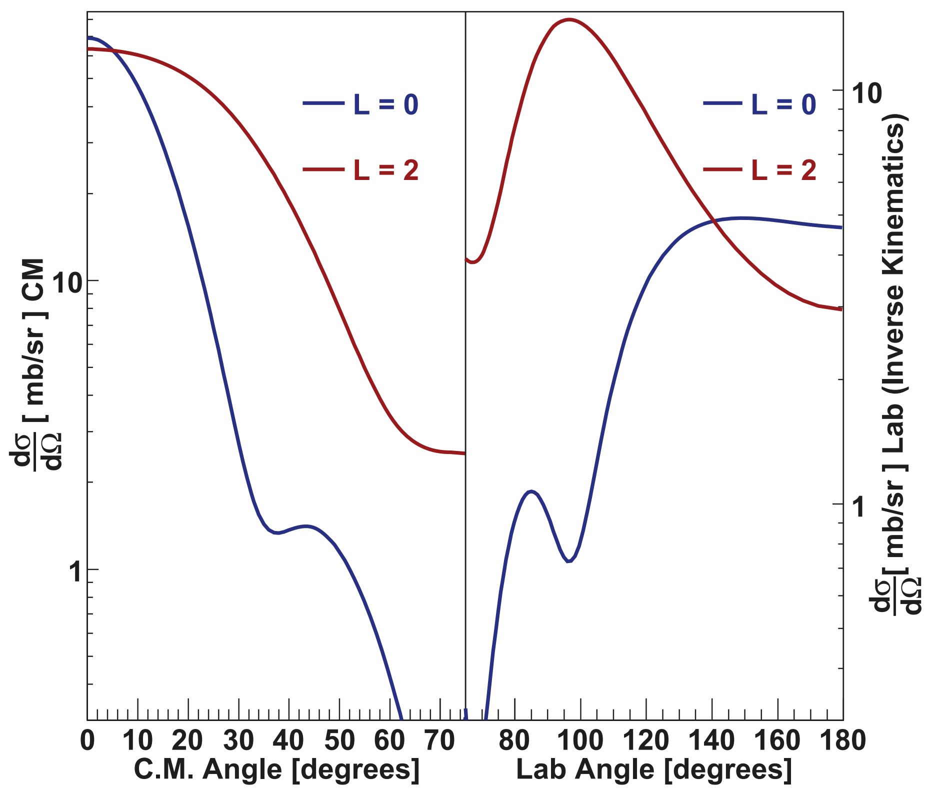

Figure 1: Left: Angular distribution for $l = 0$ and $l = 2$ neutrons for a (d,n) reaction obtained from DWBA calculation using the code DWUCK4[5] with parameters from Ref. [6]. Right: Angular distribution in laboratory angles of inverse kinematics.

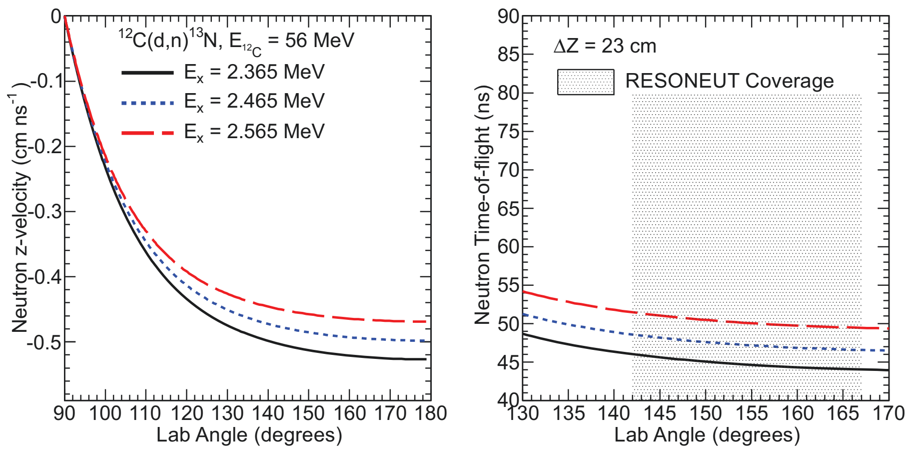

Figure 2: Left: Dependence of neutron z-velocity on laboratory angle in the ^{12}C(d,n)^{13}N reaction, populating the first excited state of ^{13}N at 2.365 MeV. Two additional kinematic curves are shown, offset by 100 and 200 keV excitation energy to illustrate the sensitivity of kinematic reconstruction. Right: TOF vs angle curves for the same ^{13}N-excitation energies, calculated for a coordinate of delta Z=-0.23 m, upstream from the target. The shaded area shows the range of angles covered by the neutron detectors.

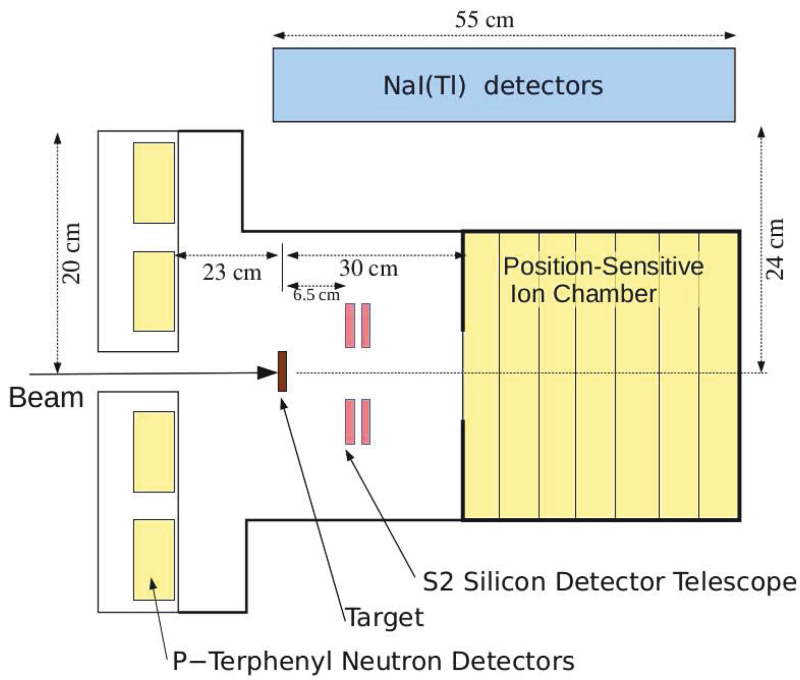

Figure 3: A schematic cross-section representation of the RESONEUT setup with its detector components (not to scale).

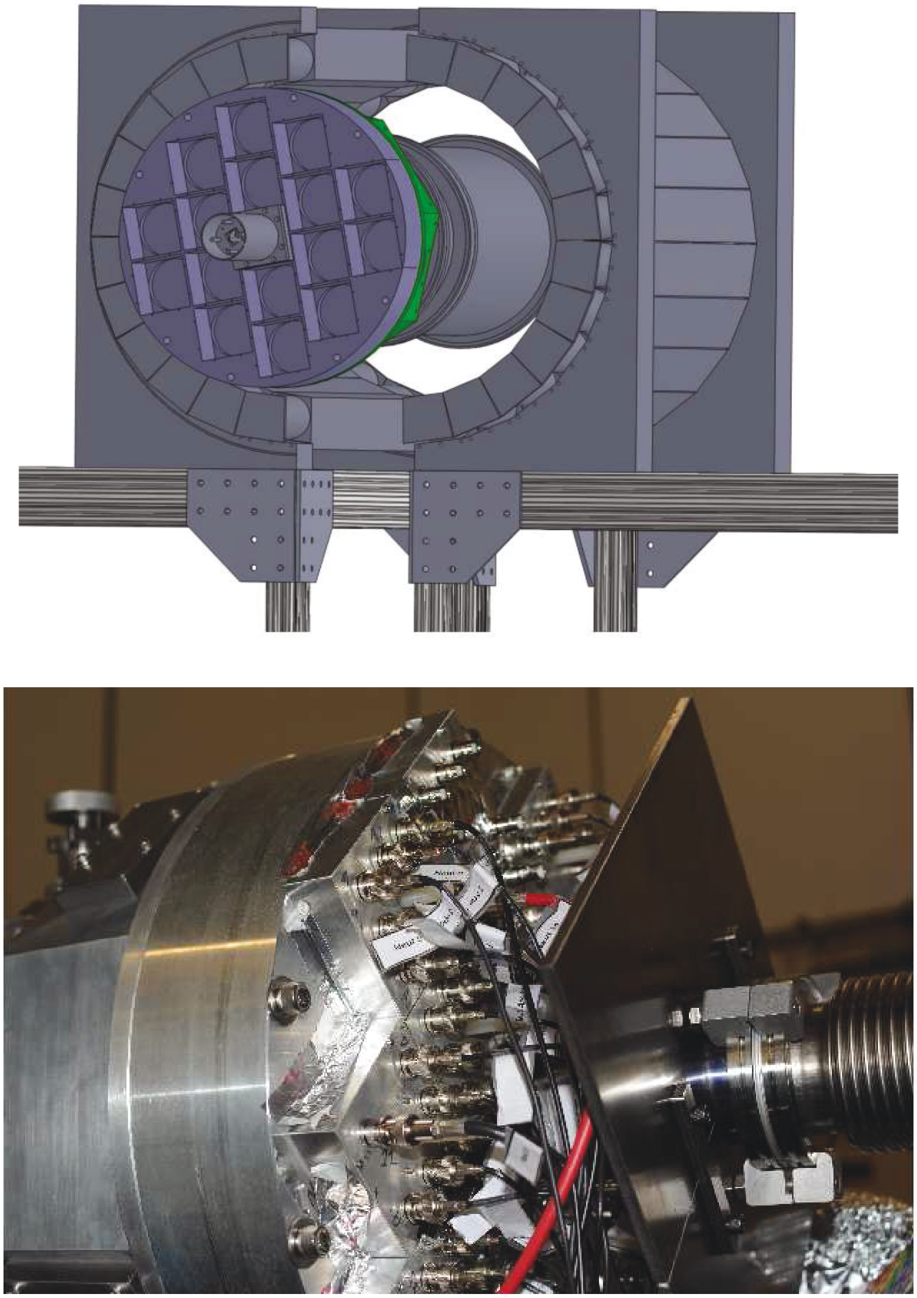

Figure 4: Top: A technical representation of the RESONEUT setup, viewed from the beam-entrance side. The vacuum chamber is surrounded by NaI-detectors, which are supported by independent frames and can be removed for access. During the experiment described here, only 20 NaI-crystals were installed. Bottom: Front-end view of the RESONEUT with the detector systems mounted.

reaction residue can strongly reduce the effects of background radiation and were realized in the setup through silicon detectors, high-efficiency γ detectors and a zero-degree gas ionization detector.

Protons emitted from resonances populated through the (d,n) reaction are emitted in forward directions with typical angles between 8 and 30 degrees with respect to the beam axis. A set of two annular double-sided silicon detectors of the Micron Semiconductor S2 design were used to detect those protons. These detectors with an inner and an outer diameter of 20 mm and 75 mm and thicknesses of 64μm and 1000μm cover the angles between 8 and 21 degrees.

In order to allow for the efficient detection of coincident γ rays, the vacuum chamber is surrounded by a 20-element position-sensitive NaI detector array, originally built for the APEX experiment [8], and later used for γ–spectroscopy of exotic nuclei [9]. The NaI(Tl) detectors are of trapezoidal shape with 55 cm length, 6 cm height and widths of 7 cm and 5.5 cm. Each detector is coupled at both ends to photomultiplier tubes, allowing to extract both the position and energy of γ rays. Note that the photo-multiplier tubes on these detector systems are magnetic-field tolerant, because of their original purpose to operate within the magnetic fields of the APEX-experiment.

Due to the inverse kinematics, the recoiling heavy nuclei emerge close to the beam axis and with energies close to the beam energy. A gas-ionization detector capable of high count rates is used to detect these recoils in coincidence and to determine the particle identity through the measurement of specific energy-loss in gas. This information is used to further discriminate between proton– and γ–decaying states in the compound system. The detector employs signal-collection fields parallel to the beam direction, with a the charge-collection distance of only 20 mm, which allows for a very stable performance at high count rates. It has been used at rates up to 60k particles per second without observable degradation in the resolution. In addition to the typical energy-loss and total energy segmentation, the first two active grids are x- and y-position sensitive and help to determine the position of the recoiling nuclei to within 2 mm resolution. The detector has been built at Louisiana State University following designs by

Chae *et al.* [10], details are described in [11] and will be the subject of another publication [12].

2.3. Neutron detector systems

The doped p-terphenyl crystals chosen for the neutron detector systems provide favorable properties for detecting neutrons of low kinetic energies through elastic scattering off the protons in the scintillator. The performance of p-terphenyl scintillation detectors has been documented in Refs. [13, 14]. P-terphenyl ($C_{18}H_{14}$) has a high density of hydrogen atoms, which provides a high neutron-scattering probability, and has a fast scintillation process, which provides excellent timing properties when coupled to suitable photomultiplier systems. It also provides substantially higher light-output than typical plastic scintillators used for neutron detection. We had considered stilbene as an alternative detector material, which has similar properties but provides slightly lower light output than p-terphenyl. ^{6}Li-loaded glass scintillators were another technology considered, but rejected, based on the relatively low detection efficiencies achievable with a compact setup and the high sensitivity to thermal neutrons.

Like some organic scintillators, p-terphenyl exhibits pulse-shape variation with the ionization density, with the fast and the slow scintillation components having time-constants of ≈ 20 ns, and ≈ 100 ns, respectively. Neutron-scattering events, which transfer energy to protons show a stronger population of the slow components than the γ-events, which transfer energy to electrons. We implemented a gated-integration technique, described in the next section, to discriminate between both types of events.

The p-terphenyl crystals used in the current setup were manufactured by Cryos-Beta Inc. The scintillator crystals of 7.1 cm diameter are encapsulated in an aluminum case with a front glass window. A photograph of a crystal is displayed in the left panel of Figure 5. In the full configuration, four detector crystals of 1.25 cm thickness occupy the locations closest to the beam axis and twelve crystals of 2.5 cm in the outer locations. During the experiments described here, only two thin-crystal detectors and 7 thick crystals were used, forming a nine-detector array.

The scintillators are coupled to "Planacon"-type photomultipliers supplied by Photonis USA. These devices utilize micro-channel plates to perform the electron-multiplication, which allows to create very compact detector systems with very good timing performance. Photographs of the photomultiplier system are displayed in the middle and the right panel of Figure 5. Typical rise times for these systems are of the order of 500 ps with a gain factor of $\approx 10^5$. The systems are well-matched to the 395 nm wavelength of p-terphenyl scintillation light. The Planacon photomultipliers used in RESONEUT have dimensions of 5 cm$\times$5 cm$\times$2.5 cm. A common signal output derived from the last stage of the MCP was used for all experiments described in this paper. In addition, the MCP-PMT provides a 64-fold segmented anode providing a position-sensitive readout, which was not used in the present set of experiments, but will be central to a further development planned for the setup. (See Figure 5).

Since the RESONEUT setup is located next to the second solenoid of the RESOLUT facility where magnetic fields of few hundred Gauss can be present, the high tolerance of MCP-PMT to external magnetic fields was another important property considered in choosing this technology.

2.4. Neutron-detector electronics and Pulse shape discrimination

The p-terphenyl detector signals are processed through a set of analog multi-channel electronics, which generate the amplified analog detector signals, the detector trigger, and gates for the gated-integration digitizers, enabling pulse-shape analysis of the detector signals to implement the neutron-γ discrimination. A circuit schematic is displayed in Figure 6. The fast output signals from the MCP systems are processed through a Mesytec MCFD module, which implements a 16 channel fast amplifier with integrated Constant-Fraction Discriminator (CFD). The module provides an amplified, analog detector signal and the logic trigger information. The analog signals are delayed by a 14-m cable before they are provided to the two 16-channel banks of a Mesytec MQDC charge-to-digital converter (QDC) through two close-by connectors on the same ribbon-cable. The full-range sensitivities of the two banks were selected to be 150 and 500 pC, respectively, and only the second bank's inputs were terminated.

The QDC-module is triggered by the "or" output of the CFD, which is suppressed in case the data-acquisition computer is busy at the time of the event. The individual-channel trigger signals from the CFD outputs are delayed by a 10-m cable before they provide the individual-channel gate inputs in series to both QDC-banks. The signal delays ensure that the common trigger for the QDC arrives at least ≈ 2 ns before the individual gate-inputs, which arrive at least ≈ 6 ns before the analog input signals in order to compensate for module-internal delays in the application of the gates. The MQDC module allows to limit the gated integration time on all channels of one bank to a software-adjustable value. This way the identical input and gate parameters to both banks can be used to implement a "short" integration gate (10 ns) and a "long" (120 ns) integration gate without generating any additional hardware signals. The first QDC bank with the higher gain setting was used with the "short" integration gate, in an effort to create a similar dynamic range in both banks.

In sequence, the individual-channel gate signals are further delayed by 200 ns, and used as the individual "stop" inputs to a CAEN V775 TDC, which is started by the common master-trigger signals. The additional 200 ns cable delay assures that neutron-timing signals arrive after a master-decision based on Silicon or NaI-detectors has been made. The additional detector-channels are analyzed in Mesytec MSCF-16 shaper-discriminator modules and CAEN V785 ADCs for energy signals and additional CAEN V775 TDCs for the time-signals. All TDC modules are started by the master trigger and stopped by a delayed instance of the respective individual signal. Another timing-reference signal is derived from the accelerator-rf reference in a separate V775 TDC channel.

The electronics described in Figure 6 analyze all neutron signals on the fastest possible time scale by using the individual neutron-detector discriminator signals, which precede all other detector signals by typically 100ns. In order to accommodate trigger conditions from the slower detectors, we created a "fast clear" logic for the charge-integrating QDC, which aborts the neutron-detector data for events which do not receive a main-trigger condition within a ≈ 200 ns time window.

An example of pulse-shape analysis obtained from the p-terphenyl scintillators is displayed in Figure 7, where the "long" integrated charge on the y-axis is correlated with the "psd" signal on the x-axis, which is the ratio of integrated charge on the long gate to that in the short gate. The parameters of pulse shape analysis of the p-terphenyl detectors were tested and optimized with a ^{252}Cf calibration source for a maximum separation to the lowest energy possible. The gate used for neutron selection is drawn generously to accept all neutron-events. For the lowest neutron energies the "psd" analysis alone is not capable of completely suppressing γ–background events, but it still contributes significantly to the selection of events in concert with the coincident detection of protons and recoiling ions.

3. Simulations, Test Experiments and Characterization of Detectors

3.1. Simulations

In order to develop a quantitative approach to guide the design process and to simulate the efficiency of the setup, we developed a Monte-Carlo simulation based on the kinematics of the (d, n) reaction and the interaction of the charged and neutral particles with the elements of the setup. The simulation code picks a randomized neutron angle in the center-of-mass system in a way that reproduces the angular distribution obtained from a DWBA calculation. The energy loss that beam-particles encounter in the target (here 520 μg / cm^2 of CD_2) was calculated using the program SRIM [16]. The beam-particle energy is chosen randomly in the interval between the incoming and outgoing energies to represent a random reaction location within the target. The chosen beam-particle energy is used to translate the neutron cm angle and energy to the laboratory system, where the interactions with detectors are described.

The interactions of a neutron with the p-terphenyl crystals are modeled as elastic scattering from either the hydrogen atoms or the carbon atoms in the p-terphenyl crystal. The neutron interaction cross sections were obtained from Evaluated Nuclear Data File(ENDF)[15]. In the simulation, only the events which result in an elastic scattering with hydrogen atoms yield a scintillation signal detectable above the threshold, while scattering on carbon (for the case of low energy neutrons) yield only a net deflection of the neutrons and no detectable scintillation. All interactions of a single neutron within the scintillator are summed up to decide if a signal above threshold is generated. Also included are the scattering processes in the material of the vacuum chamber (see Figure 4), which can lead some scattered neutrons reaching the detector crystals.

Figure 8 displays a spectrum extracted from a simulation of the reaction $^{12}\mathrm{C(d,n)}^{13}\mathrm{N}$ in inverse kinematics, for the states of interest and additional states to show the expected detector response over a range of excitation energies. In the simulation, as in the experimental data analysis, the reaction Q-value is calculated from the neutron energy and the neutron emission angle using the expression -

$$Q = E_n[1 + \frac{m_n}{m_{N13}}] - E_{Beam}[1 - \frac{m_{Beam}}{m_{N13}}] - \frac{2}{m_{N13}}\sqrt{E_{Beam}E_n m_n}cos(\theta_n) \quad (1)$$

, where E_n is the neutron-energy reconstructed from the distance between target and detector and the measured time of flight.

The simulation allows us to determine the major factors limiting the energy resolution of reconstructed Q-values. For the state at 2.365 MeV the dominant contribution to the reconstructed Q-value peak width comes from the thickness of the detector(≈150 keV). Other sources include the target thickness (≈90 keV), kinematic variation across a single detector(≈ 30 keV) and the 1.6 ns beam bunch width (≈ 50 keV), resulting in a FWHM resolution of around 180 keV as an Gaussian-peak width estimate. The slightly asymmetric peak shape, stemming from scattering on materials surrounding the detectors, leads to an additional broadening and a effective FWHM of 200 keV.

3.2. Determination of neutron signal response

The efficiency of the detector systems depends critically on the achievable low-energy threshold, which enters as a free parameter into the simulation and has to be determined experimentally. Details of the determination are given in Section 3.4. Like many organic scintillators, the p-terphenyl crystals show a substantially different response to energy deposited by γ-radiation or neutrons, which transfer energy to electrons or protons, respectively, and cause greatly different excitation densities in the scintillator crystal. This effect allows for the above-described pulse-shape discrimination between neutron– and γ–induced events and is also creating a different proportionality factors between the energy deposited and the amount of scintillation light produced. For a typical plastic scintillator, this ratio of scintillation light intensity per energy deposited (EE/EP) through energetic electrons or protons is around 10 to 1.

The calibration of the scintillator response to γ rays from sources with known γ–energies is straightforward; We use sources of ^{241}Am, with its 26.3- and 59-keV lines, and ^{137}Cs, which has a 667 keV line, detected as its Compton-escape edge at 475 keV. The position of the Compton edge is extracted by folding a theoretical shape of the Compton-edge with the detector-resolution and fit the resulting shape to the experimental spectrum.

The pulse-height calibration function of the scintillator is plotted in Figure 9 as a function of the γ-ray energy, which is in the following identified as "electron-equivalent energy". For detectors with the lowest electron-detection thresholds, the Am-241 26.3 keV line partially merge with the high energy tail of a peak centered close to $\approx$ 10 keV which is originating from the Compton edge of the 59 keV γ-ray. For each of the 2.5-cm-thick crystals, consistent resolutions are observed for the ^{241}Am line and the ^{137}Cs Compton edge, which are 35(1)% and 18(1)% respectively. Resolutions of 30(1)% and 17(1)%, respectively, are extracted for the 1/2" thick crystals. These resolutions are slightly worse than those reported in Refs. [13] and [14].

The second task is to find the response of the scintillators to neutrons of known energies. Since mono-energetic neutron sources are not available, we used the continuous spectrum emitted in the spontaneous fission decays from a ^{252}Cf source and a time-of-flight measurement to determine the neutron-energies event-by-event. With the ^{252}Cf source located at the target position of the RESONEUT setup, we recorded coincidence events involving two p-terphenyl detectors and the relative coincidence time. The delayed events correspond to coincident detections of one neutron and one γ–ray, where the neutron time of flight was identified with the delay time. The time of flight (TOF) is extracted by subtracting the gamma-ray time of flight (around 1 ns) from the coincidence time.

Figure 10 displays the two-dimensional histogram relating the measured time of flight and the detector pulse height, calibrated in electron-equivalent energy. The histogram shows events from coincidence detections of two γ–rays around 1 ns time-of-flight values. The pulse-height of these events is measuring the energy of recoiling protons and ranges continuously from the full energy of the neutron to zero. Figure 11 shows the relation of the "electron-equivalent" energy as a function of the neutron time-of-flight, including data points obtained from the experiment described in the following section. The full-energy pulse heights detected for a given neutron energy are consistently lower by a factor 5.5±1.5 as compared to the corresponding "electron-equivalent" pulses.

3.3. Measurement of $^{12}C(d,n)^{13}N$ reaction

In order to determine the performance of the detector systems for the neutron-spectroscopy of low-lying proton resonances, we performed an experiment with the $^{12}\mathrm{C}(\mathrm{d,n})^{13}\mathrm{N}$ reaction in inverse kinematics and conditions similar to the radioactive-beam experiments for which RESONEUT was developed. In the experiment, beams of ^{12}C at 4.4 and 4.66 MeV/u were bombarding a deuterated polyethylene foil of 520 $\mu g/\mathrm{cm}^2$ at the target position of the RESONEUT setup. The beam particles were pulsed to short bunches of around 1.6 ns duration, separated by 82.5 ns and accelerated by the FN Tandem accelerator at the John D. Fox Laboratory of Florida State University. During this experiment, nine p-terphenyl detectors were present.

In the $^{12}C(d,n)^{13}N$ reaction, the $1/2^-$ ^{13}N ground state and the $1/2^+$ first excited state at 2.365 MeV are strongly populated via $l = 1$ and $l = 0$ proton transfer, respectively. The first excited state also lies 422 keV above the proton separation energy and thus decays exclusively by proton emission. The excited $3/2^-$ state at 3.502 MeV also decays by proton emission and is seen in the proton spectrum, but the corresponding neutrons are below the detection threshold.

3.4. Determination of neutron-detector energy thresholds

The kinematic properties of this reaction for low-lying proton resonances have been discussed in previous paragraphs. For events populating the first excited state, the 4.4 MeV/u and 4.66 MeV/u accelerated beams provided neutrons of energies around 130 keV and 210 keV respectively, within the angles covered by the p-terphenyl detectors. These events also generate protons from the resonance decay, emitted in forward directions, where they are detected with the annular silicon detectors. Detection of signals in a silicon-detector or a p-terphenyl detector were used as triggers for the data acquisition system. The fraction of proton-based events with coincident neutrons allow for an independent measurement of the neutron-detection efficiency and a verification of the simulation. For the case of ground state population we expect to see only the neutron and hence the data is collected with a neutron-singles trigger.

The time-of-flight parameter is determined relative to the periodic accelerator rf-reference, which is measured in a separate channel of a CAEN V775 TDC module (see Sect. 2.4). The accelerator beam is bunched and chopped at 12.125 MHz frequency, which corresponds to a 82.5 ns bunch-separation period. The TOF signal is reconstructed in the analysis by subtracting the accelerator RF time from the individual particle detection times. In the resulting TOF spectra the "zero" time reference is determined through the observation of prompt γ–rays.

Figure 12 shows an example of the proton-gated TOF spectra obtained from the runs with the 4.66 and 4.35 MeV/u beam energies. Since the neutron-energies detected in the lower-energy run approach the detection thresholds of individual detectors, the observed yield at the lower energy is very sensitive of the detection-threshold parameter, which was adjusted to reproduce the experimental yield. It was verified that the extracted thresholds, which are listed in Table 1, consistently reproduce the data from both beam-energies and are consistent with the γ–detection thresholds obtained separately.

The energy-dependence of detection efficiencies for three detector systems, calculated by the Monte-Carlo simulation is displayed in Figure 13, showing the effect of crystal thickness and the sensitivity to the low-energy detection threshold of the different detection systems. The limit in achieving low thresholds are determined by individual properties of the crystals, electronic noise, the noise-level of dark current in the MCP-PMT and the stability of the electronic channels associated with signal processing. Generally, we were able to achieve lower thresholds from the thinner type of crystals.

Det. No.	1	2	3	4	5	6	7	8	9
Threshold (keV)	70	65	65	85	90	105	105	105	97

Table 1: Extracted neutron-energy thresholds in keV for the RESONEUT detectors. Detectors 2 and 3 are crystals with 1.25-cm thickness, the others are 2.5 cm thick.

3.5. Excitation spectra, resolution and efficiency

The extracted TOF spectra collected with the 4.66 MeV/u beam energy are displayed in Figure 14, along with the results of the Monte Carlo simulation. In the top panel, the TOF spectrum gated on coincident proton-emission is shown, which is dominated by one peak from the first excited ^{13}N state at 2.365 MeV with a resolution of around 200 keV FWHM.

The lower panel of Figure 14 shows the analogous spectrum of neutron-singles events with a peak corresponding to the population of the ^{13}N ground state. Here, in an effort to reduce the background events, an additional requirement for the signal amplitude to be larger than 45 keVee was applied. The poorer statistics stem from the reduced efficiency of our detectors for neutrons of around 750 keV energy and the fact that the neutron-singles events were only recorded for a half-hour run during the experiment. In both cases the simulated peak-shapes show a very good fit, including the detector resolution and a slightly asymmetric peak shape with a tail towards longer flight times, which is caused by scattering off the vacuum chamber material into the detectors. In the simulations of both spectra we used the relative cross section for the ground state and the 2.365 MeV state from Schelin *et al* [6]. The reproduction of the peak size in the upper- and lower-panel spectrum also implies that the absolute detection efficiency is well reproduced over the relevant energy range.

The Q-value spectra of the ^{12}C$(d,n)^{13}$N reaction is reconstructed by calculating the neutron energy from the TOF data using the flight path towards the center of the respective detector with Eq. 1. The excitation energy is then created by subtracting the reaction Q-value from ground-state Q-value (-0.281 MeV). The resulting spectrum reconstructed from all detectors is shown in Figure 15. The observed peak shape is consistent with the Monte-Carlo simulation and shows a resolution of 200 keV FWHM.

E_{res} (keV)	E_n (keV)	Q-value resolution (keV)	Average detector efficiency	Total detection efficiency
100	200	226	0.45	0.018
300	160	200	0.40	0.015
500	130	180	0.31	0.010
700	100	170	0.20	0.005

Table 2: Summary of performance characteristics of the RESONEUT neutron detection systems, calculated using the Monte-Carlo simulation for the ^{12}C(d, n)^{13}N reaction at 4.67 MeV/u and four hypothetical resonance energies. Total detection efficiency is the ratio of detected events to the total events in the simulation.

A summary of the current performance of the RESONEUT detector system, based on the parameters extracted from the Monte-Carlo simulation describing the experiment is given in Table 2. From the experience gained in the first round of experiments with RESONEUT, several areas of improvement were identified. An obvious modification comes from the addition of seven detector systems to occupy all available slots in the vacuum chamber as funds become available. The low-energy detection thresholds of the existing detector systems were limited by problems with some of the PMT-bases and the lack of preamplifier modules close to the detector systems. We expect that neutron-detection thresholds of 50 keV can be achieved by optimizing the relevant electronics components. Using the simulation developed for the current setup, we expect to arrive at a total detection efficiency of around 5% for the typical (d,n) events associated with low-lying resonances.

Finally, a new multi-channel gated-integration data acquisition system is being developed with the aim to extract the segmentation information from the MCP-PMT. The spatial light-distribution will be analyzed in an effort to extract information about the depth of the neutron detection within the p-terphenyl crystal. This ability would lead us expect a higher reconstructed energy resolution, since the detector crystal thickness is an important limiting factor for the spectral resolution achieved in the present experiments.

4. Summary

We developed and characterized the compact detector setup RESONEUT with the capability to detect low-energy neutrons with high efficiency and enable experiments using the (d,n) reaction in inverse kinematics for an efficient spectroscopy of low-lying proton resonances. The most prominent properties include a high efficiency per detector, up to 55% for some detector systems. The setup includes the ability to detect coincident light charged particles using DSSD annular silicon detectors, heavy ion reaction residues in a gas-ionization chamber and γ–rays with a barrel of NaI-detectors.

This setup is being used for experiments with radioactive and stable beams at the RESOLUT radioactive beam facility at the Florida State University. Experiments performed on radioactive beams include the ^{19}Ne(d,n)^{20}Na reaction [17] and ^{25}Al(d,n)^{26}Si [18]. The first successful neutron-spectroscopy experiment with a radioactive beam, which determined asymptotic normalization coefficients in the ^{17}F(d,n)^{18}Ne reaction has been submitted for publication [7].

Acknowledgments

RESONEUT was developed as a joint project between University of North Florida and the Florida State University, funded by National Science Foundation grant no. PHY-1126345, with partial support by the U.S. Department of Energy under grant no. de-fg02-02er41220 and from NSF under grant phy1401574. We acknowledge the excellent support by P.A. Barber, B. Schmidt and D. Spingler at the John D. Fox accelerator laboratory and R. Boisseau and J. Aragon at the instrument shop for the outstanding craftsmanship in the fabrication of the RESONEUT setup. We also acknowledge Mesytec Inc. for making available an MQDC module prototype for the development of this experiment.

References

[1] S. Engel, D. Hutcheon, S. Bishop, L. Buchmann, J. Caggiano, M.L. Chatterjee, A.A. Chen, J. D'Auria, D. Gigliotti, U. Greife, D. Hunter, A. Hussein, C.C. Jewett, A.M. Laird, M. Lamey, W. Liu, A. Olin, D. Ottewell, J. Pearson, C. Ruiz, G. Ruprecht, M. Trinczek, D. Ottewell, C. Vockenhuber and C. Wrede, *Commissioning the DRAGON facility at ISAC*, Nucl. Instrum. Methods A 553 491 (2005)

[2] Georg P. A. Berg, Jeff C. Blackmon, Manoel Couder, U. Greife, F. Montes, K. Ernst Rehm, Hendrik Schatz, Michael S. Smith, Michael Wiescher, and Al Zeller, *Design of a New Recoil Separator for Measurements of Radiative Capture Reactions in Astrophysics* AIP Conference Proceedings 1269, 445 (2010); doi: 10.1063/1.3485196

[3] M.H. Macfarlane and J.B. French. Stripping reactions and the structure of light and intermediate nuclei. Review of Modern Physics 32, 567 (1960).

[4] I. Wiedenhover, L.T. Baby, D. Santiago-Goanzalez, A. Rojas, J.C. Blackmon G.V. Rogachev, J. Belarge, E. Koshchiy, A.N. Kuchera, L.E. Linhardt, J. Lail, K.T. Macon, M. Matos, and B.C. Rascol. Studies of exotic nuclei at theRESOLUT facility of Florida State University. Proceeding of Fifth Internationa Conference of Fission and Properties of Nuetron-rich Nuclei, World Scientific 2012 (114-151)

[5] P.D. Kunz. DWUCK4, http://spot.colorado.edu/kunz/DWBA.html.

[6] H.R Schelin, E. Farrelly Pessoa, W. R. Wylie, E. W. Cybulska, K. Nakayama, L. M. Fagundes and R. A. Douglas, *The* $^{12}C(d,n)^{13}N$ *reaction between Ed=7.0 and 13.0 MeV.* Nuclear Physics A, 414(1):67-84, 1984.

[7] S.A. Kuvin, J. Belarge, L.T. Baby, J. Baker, I. Wiedenhöver, P. Höflich, A. Volya, J.C. Blackmon, C.M. Deibel, H.E. Gardiner, J. Lai, L.E. Linhardt, K.T. Macon, E. Need, B.C. Rasco, N. Quails, K. Colbert, D.L. Gay, N. Keeley, *Measurement of* $^{17}\mathrm{F(d,n)}^{18}\mathrm{Ne}$ *and its Impact on the Astrophysical* $^{17}\mathrm{F(p,}\gamma)^{18}\mathrm{Ne}$ *Reaction*, *to be published*

[8] N.I. Kaloskamis, K.C. Chan, A.A Chishti, J.S. Greenberg, C.J. Lister, S.J. Freedman, M. Wolanski, J. Last and B. Utts. *The trigger detector for APEX: An array of position sensitive NaI(Tl) detectors for the imaging of positrons from heavy-ion collisions.* Nuclear Instruments and methods in Physics Research A, 330(3),447-457, 1993.

[9] B.C. Perry, C.M. Campell, J.A. Church, D.C. Dinca, J. Enders, T. Glassmacher, Z. Hu, K.L. Miller, W.F. Mueller and H. Oliver. *A high-efficiency NaI(Tl) detector array with position sensitivity for experiments with fast exotic beams.* Nuclear Instruments and Methods in Physics Research A505, 85-88, 2003.

[10] K.Y. Chae, S. Ahn, D.W. Bardayan, K.A. Chipps, B. Manning, S.D. Pain, W.A. Peters, K.T. Schmitt, M.S. Smith, and S.Y. Strauss. *Construction of a fast ionization chamber for high-rate particle identification.*, Nuclear Instruments and Methods in Physics Research Section A: 751:6-10 (2014)

[11] Jianping Lai, *A Direct Study Of The* $^{20}Ne(\alpha,p)^{23}Na$ *Reaction With The Helical Orbit Spectrometer (HELIOS)*, Ph.D. Thesis, Department of Physics and Astronomy, Louisiana State University, December 2016

[12] J. Lai et al, Nuclear Instruments and Methods in Science Research. Under review, 2017

[13] C. Matei, F.J. Hambsch and S. Oberstedt. Proton light output function and neutron efficiency of a p-terphenyl detector using ^{252}Cf source. Nuclear Instruments and Methods in Physics Research A, 676: 135-139, 2012.

[14] A. Sardet, C Varignon, B. Laurent, T. Grainer, A Oberstedt. Nuclear Instrruments and Methods. A 792 (2015) 74-80.

[15] M.B Chadwick. ENDF/B-VII.1 Nuclear Data for Science and Technology: Cross Sections, Covariances, Fission Product Yields and Decay Data. Nucl. Data Sheets, 112:2887-2996, 2011.

[16] J.F. Ziegler. SRIM-2003, Nuclear Instruments and Methods B, 219-220(2004) 1027-1036.

[17] J. Belarge, S.A. Kuvin, L.T. Baby, J. Baker, I. Wiedenhöver, P. Höflich, A. Volya, J.C. Blackmon, C.M. Deibel, H.E. Gardiner, J. Lai, L.E. Linhardt, K.T. Macon, E. Need, B.C. Rasco, N. Quails, K. Colbert, D.L. Gay, N. Keeley, *Experimental investigation of the* $^{19}\mathrm{Ne}(\mathrm{p},\gamma)^{20}\mathrm{Na}$ *reaction rate and implications for breakout from the hot CNO cycle*, Physical Review Letters **117**, 182701 (2016)

[18] J. Baker, *Measurement of the* $^{25}Al(d,n)^{26}Si(p)$ *reaction at RESOLUT*, Ph.D. thesis, Physics Department, Florida State University, January 2016

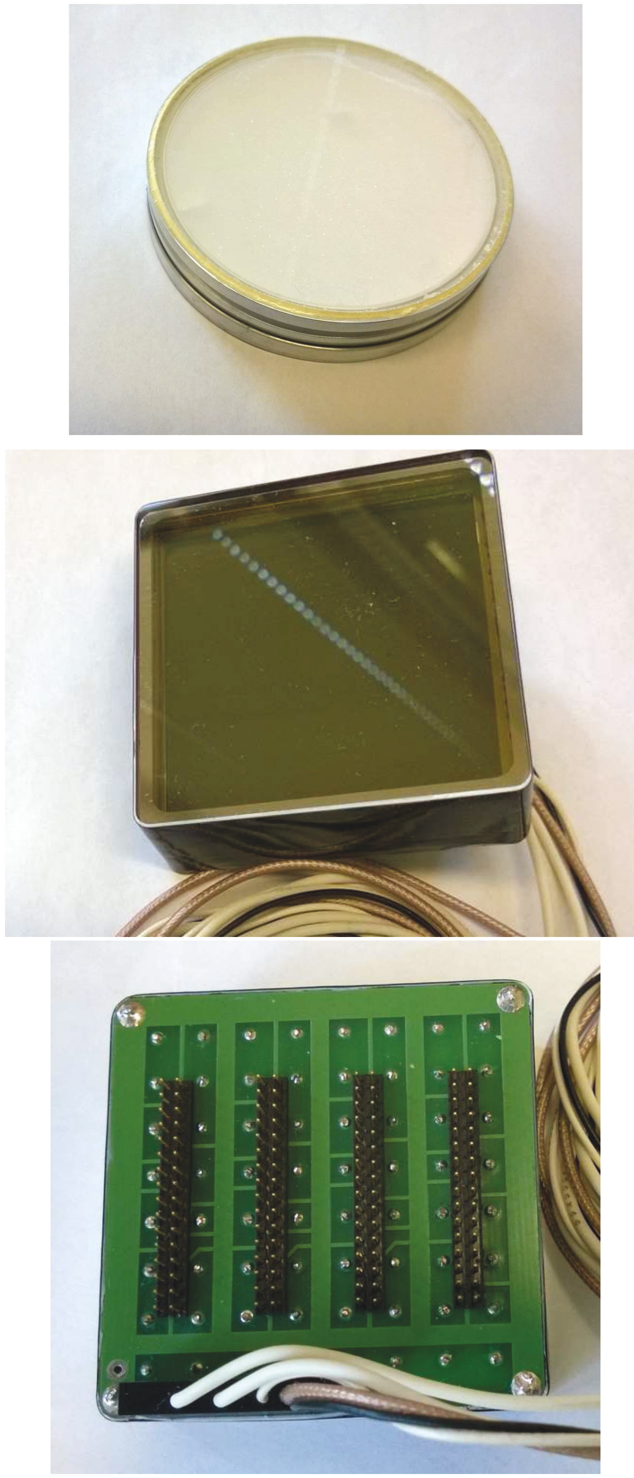

Figure 5: Left: p-terphenyl crystal contained in aluminum-glass capsule, Middle: Front view of the Planacon MCP-PMT, Right: Rear view of the MCP-PMT with connectors.

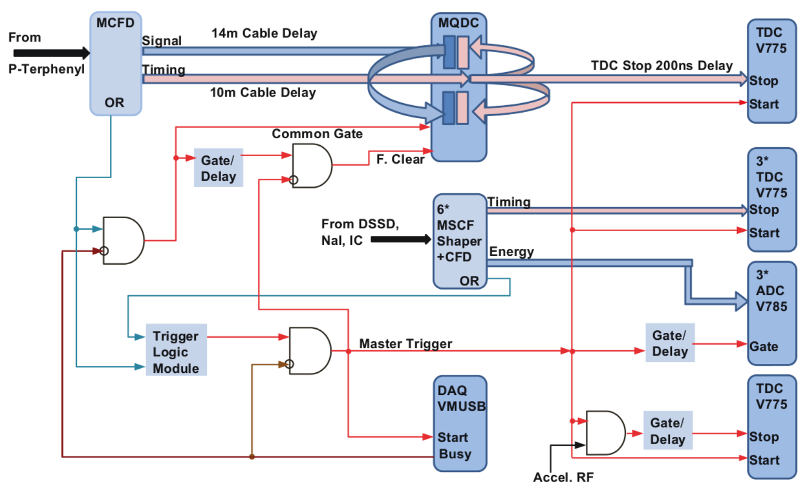

Figure 6: A schematic diagram of the signal electronics used for the neutron-detector systems of RESONEUT. (See text.)

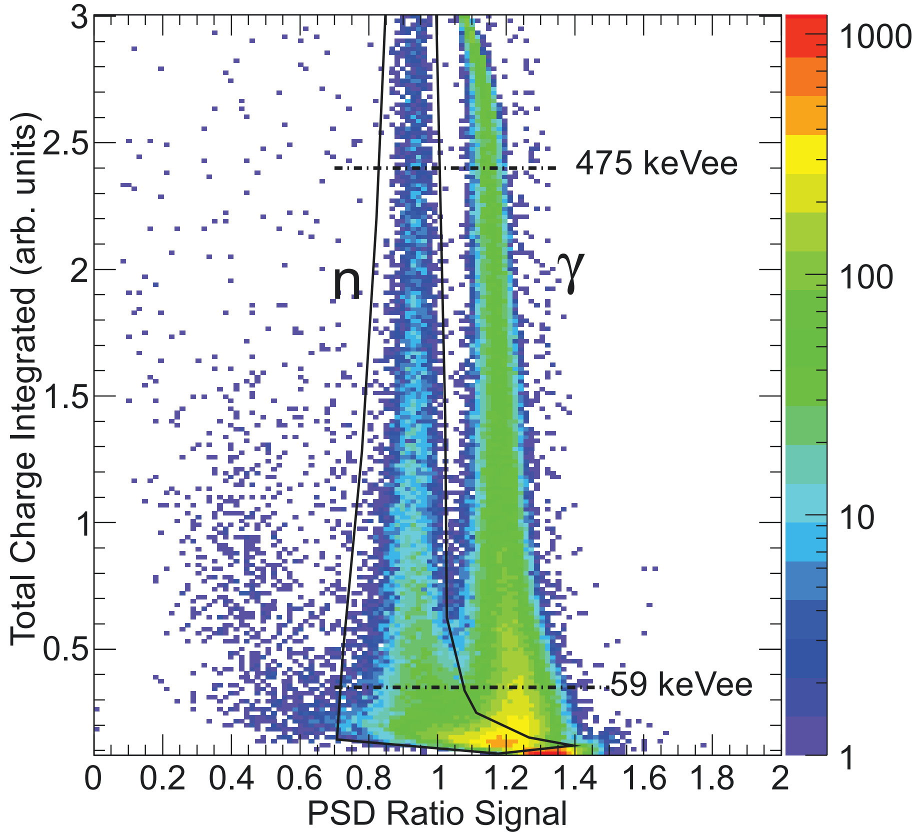

Figure 7: A histogram representing pulse-shapes obtained with a RESONEUT detector and neutrons and gamma rays emitted from a ^{252}Cf source. The vertical axis represents integrated charge in the "long" gate and the horizontal axis represents the ratio of charges in the "long" gate to the "short" gate. Because of the higher gain of the "short"-gate QDC bank, the ratios vary around unity. Also shown is the gate used for neutron selection, which is drawn to not suppress any neutron-events from the analysis at the cost of allowing additional background from γ rays at low energies.

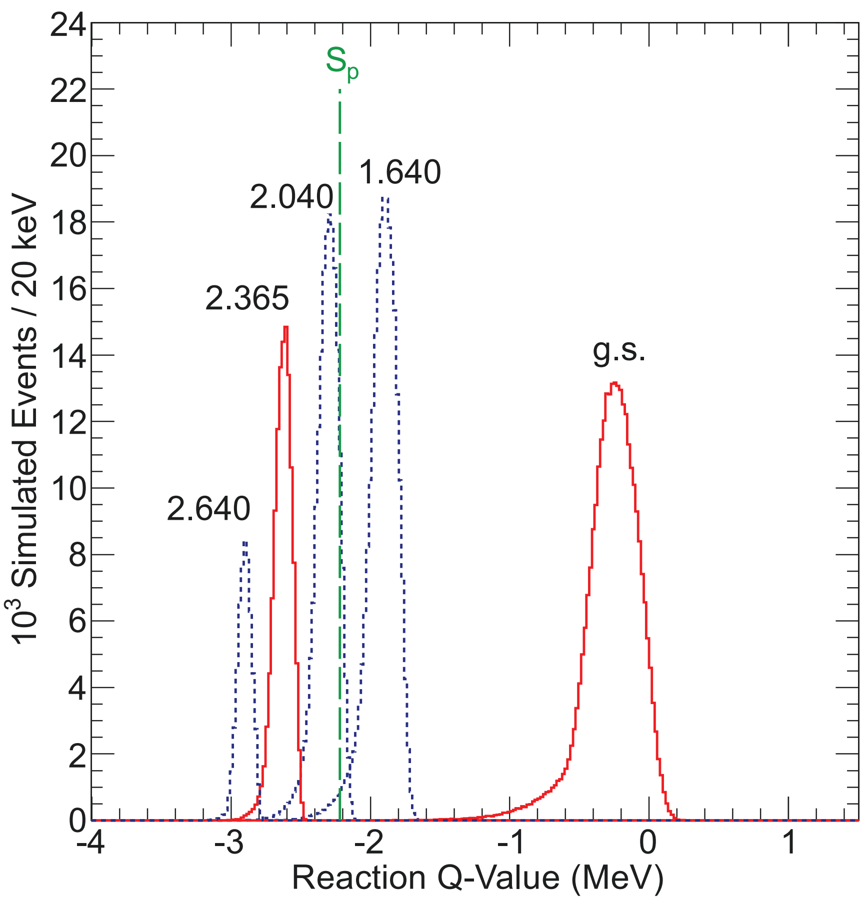

Figure 8: Q-value spectrum obtained from the Monte-Carlo simulation of RESONEUT detector system and the $^{12}C(d,n)^{13}N$ reaction, represented by peaks with red lines. For the purpose of comparison, additional hypothetical peaks are shown with dashed blue lines are closely spaced simulated levels to show the response characteristics of the setup.

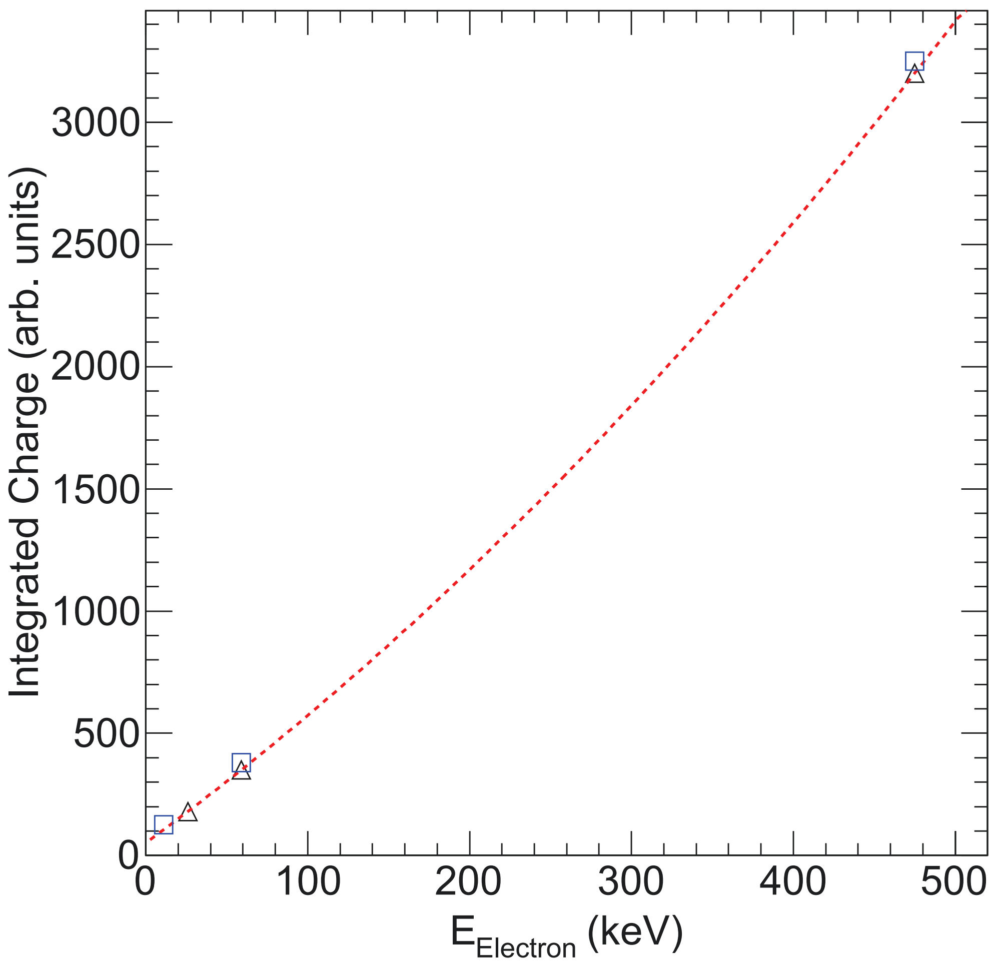

Figure 9: Representation of detector signals in electron-equivalent energy obtained from two RESONEUT detector systems. The data points correspond to the 26 keV and 59 keV photo peaks from ^{241}Am and the 475 keV Compton edge of the 667 keV γ ray from ^{137}Cs. The red line is second-order polynomial fit to the data.

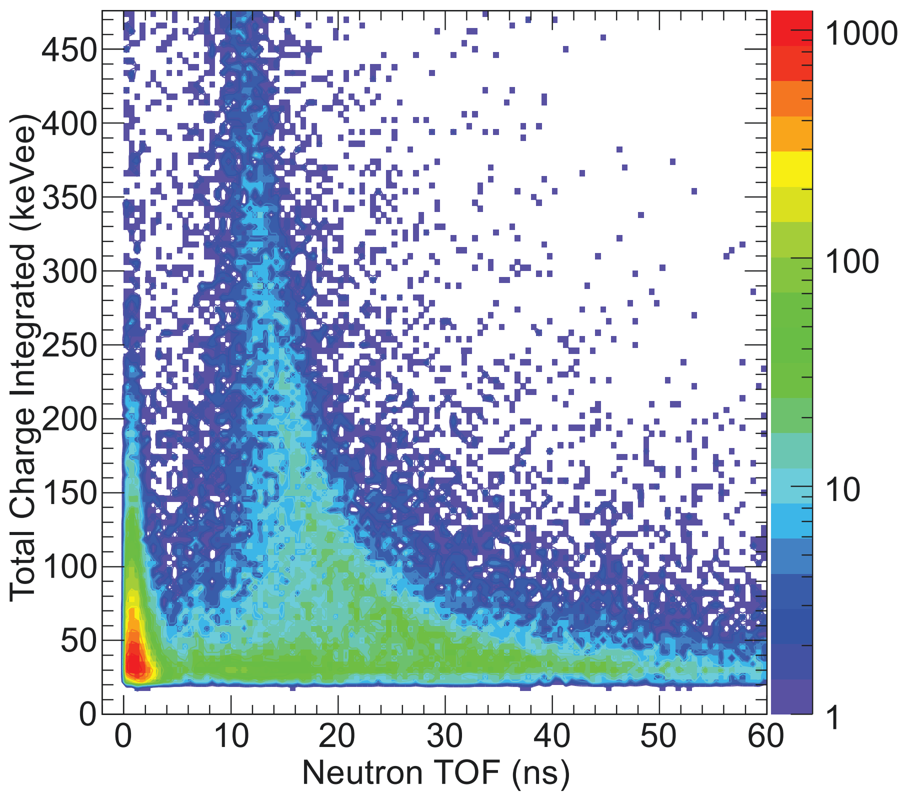

Figure 10: A two-dimensional histogram of detected charge in electron-equivalent energy units vs. time of flight of neutrons from ^{252}Cf source from a single p-terphenyl crystal (see text).

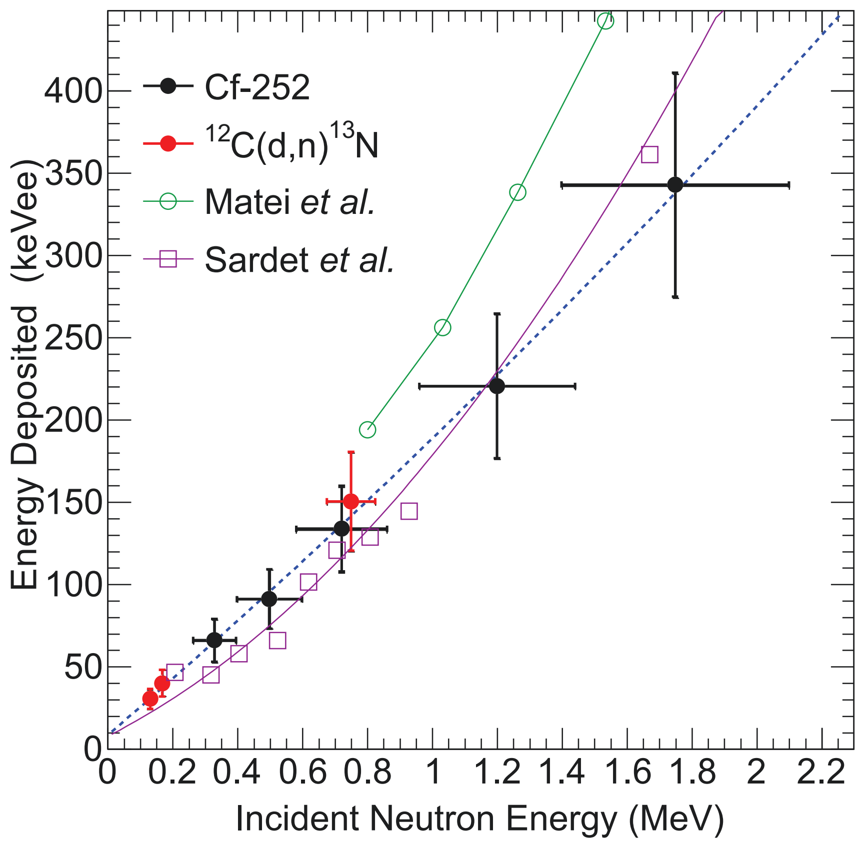

Figure 11: Incident neutron energy vs maximum scattering energy expressed in units of electron equivalent energy (keVee). The Cf-252 data represents the upper limit of the charge distributions with the associated uncertainties. The x-errors represent the uncertainty in the neutron energies. Red data points were extracted in a similar manner from in-beam spectra of the ^{12}C(d,n)^{13}N experiment. The blue line is a linear fit to the data. For comparison, equivalent data from Ref. [13] and ref. [14] are shown.

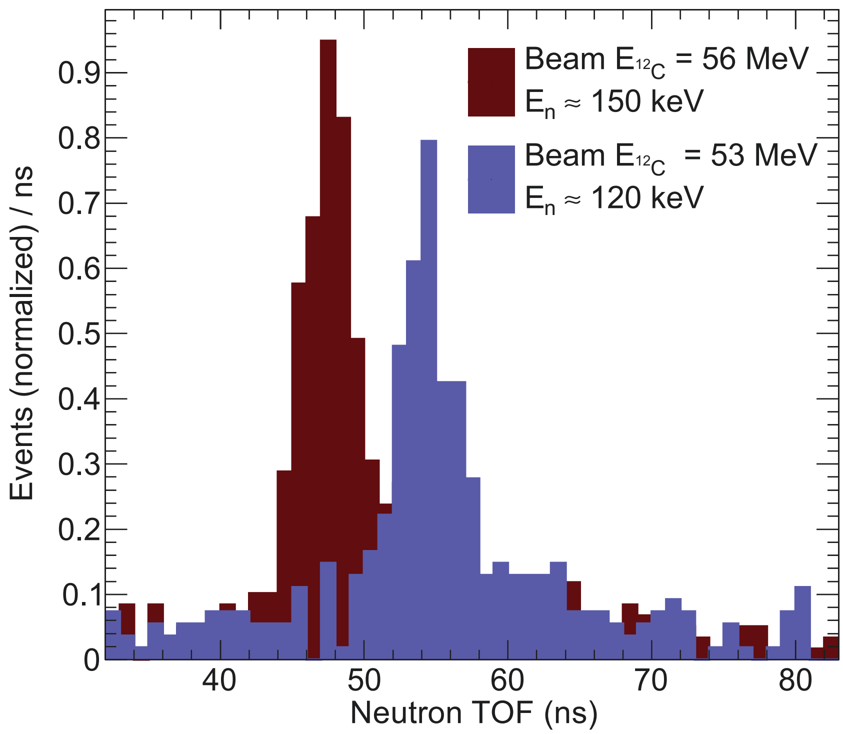

Figure 12: Neutron TOF spectrum for populating the $\frac{1}{2}^+$ state obtained through two different beam energies. The effect of neutron-detector thresholds are reflected in the lower statistics in the TOF peak from the lower beam energy. The data presented in this picture is for one of the inner detectors where the neutron energy is 120 keV and 150 keV respectively, for the two beam energies. The spectra are normalized to the peak area of the protons detected in coincidence.

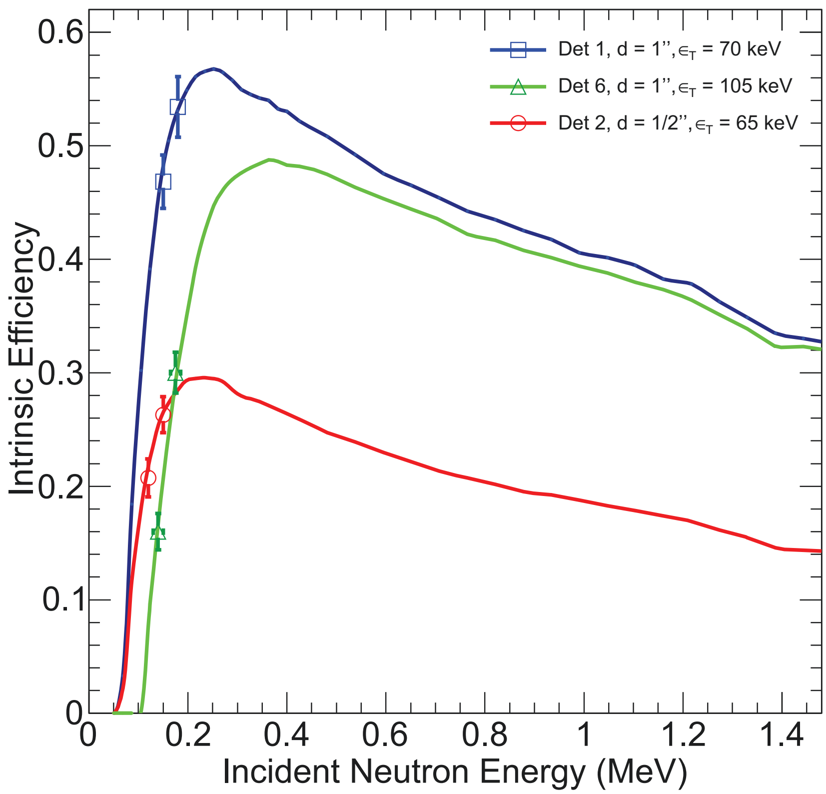

Figure 13: Intrinsic efficiency curves extracted from the Monte-Carlo simulation for three different neutron detector systems. The red curve represents for a 1.25 cm thick crystal, the other two are for 2.5 cm thick crystals. The detection thresholds determined for each of the crystals are also listed. The data points are the respective detector efficiencies in the $^{12}C(d,n)^{13}N$ experiment.

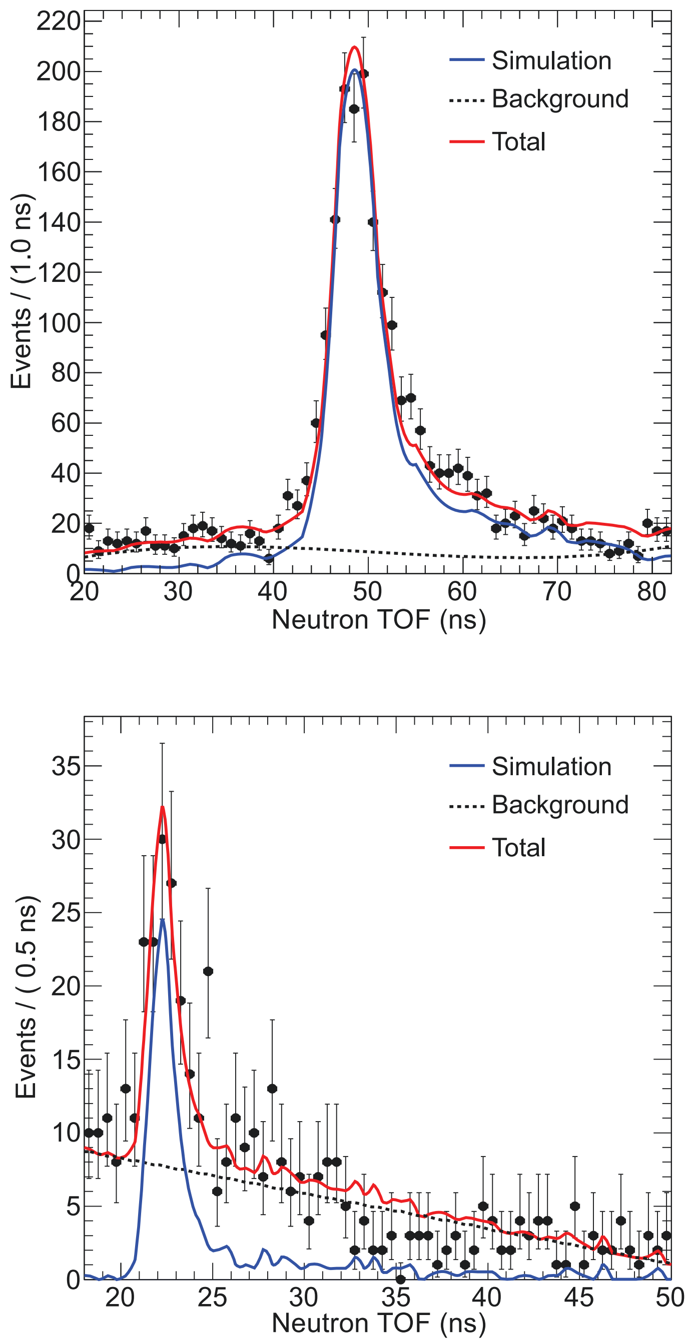

Figure 14: Top: Experimental time-of-flight spectrum of neutrons from the ^{12}C(d,n)^{13}N reaction after populating the excited state at 2.365 MeV, detected in a 1.25 cm thick crystal, Bottom: Time of flight spectrum for the same reaction, gated in addition on detector-charges above 45 keVee. The spectrum shows a peak representing population of the ^{13}N ground state, for which the per-crystal detection efficiency is $\approx$ 17%.

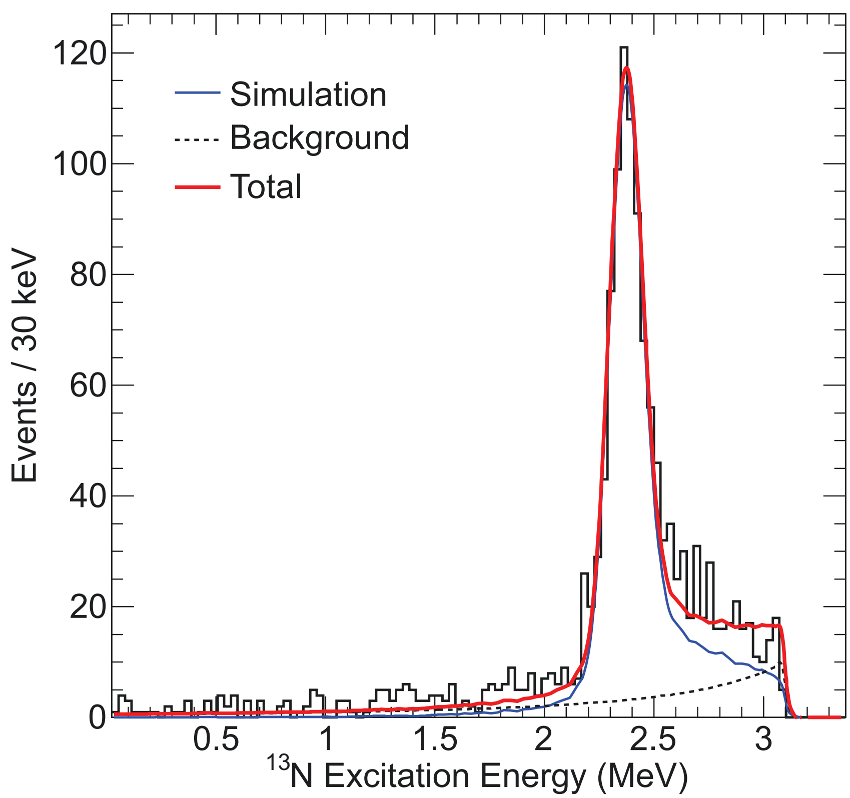

Figure 15: The reconstructed excitation energy spectrum for the ^{13}N nucleus using signals from all neutron detectors. The spectrum is compared to the results of a Monte-Carlo simulation, added to a polynomial background hypothesis.